Naval Research Laboratory

Washington, DC 20375-5000 NRL Memorandum Report 5853 September 12, 1986

Effects of Cathode Surface Roughness on the Quality of Electron Beams

Y. Y. LAU

Plasma Theory Branch
Plasma Physics Division

This work is partially sponsored by the Office of Naval Research and the Defense Advanced Research Projects Agency under Contract #5483.

AD-A173189

SECURITY CLASSIFICATION OF THIS PAGE

REPORT DOCUMENTATION PAGE

1a. REPORT SECURITY CLASSIFICATION UNCLASSIFIED	1b. RESTRICTIVE MARKINGS
2a. SECURITY CLASSIFICATION AUTHORITY	3. DISTRIBUTION/AVAILABILITY OF REPORT Approved for public release; distribution unlimited.
2b. DECLASSIFICATION/DOWNGRADING SCHEDULE	
4. PERFORMING ORGANIZATION REPORT NUMBER(S) NRL Memorandum Report 5853	5. MONITORING ORGANIZATION REPORT NUMBER(S)
6a. NAME OF PERFORMING ORGANIZATION Naval Research Laboratory 6b. OFFICE SYMBOL (If applicable) Code 4790	7a. NAME OF MONITORING ORGANIZATION
6c. ADDRESS (City, State, and ZIP Code) Washington, DC 20375-5000	7b. ADDRESS (City, State, and ZIP Code)
8a. NAME OF FUNDING/SPONSORING ORGANIZATION DARPA 8b. OFFICE SYMBOL (If applicable)	9. PROCUREMENT INSTRUMENT IDENTIFICATION NUMBER
8c. ADDRESS (City, State, and ZIP Code) Arlington, VA 22209	10. SOURCE OF FUNDING NUMBERS PROGRAM ELEMENT NO. 62702E; PROJECT NO.; TASK NO.; WORK UNIT ACCESSION NO. DN155-384

11. TITLE (Include Security Classification)
Effects of Cathode Surface Roughness on the Quality of Electron Beams

12. PERSONAL AUTHOR(S)
Lau, Y. Y.

13a. TYPE OF REPORT	13b. TIME COVERED	14. DATE OF REPORT (Year, Month, Day)	15. PAGE COUNT
Interim	FROM _____ TO _____	1986 September 12	39

16. SUPPLEMENTARY NOTATION This work is partially sponsored by the Office of Naval Research and the Defense Advanced Research Projects Agency under Contract #5483.

17. COSATI CODES		
FIELD	GROUP	SUB-GROUP

18. SUBJECT TERMS (Continue on reverse if necessary and identify by block number)
Electron beam quality; Beam emittance; Beam brightness; Cathode surface roughness

19. ABSTRACT (Continue on reverse if necessary and identify by block number)

The effects of the roughness of the cathode surface on the emittance of an electron beam are examined. Tentative scaling laws are suggested which yield the bounds on the beam emittance due to surface roughness for both temperature limited and space charge limited regimes. These formulas are found to be consistent with numerical integration of electron trajectories over a wide range of parameters. In general, roughness-induced beam emittance may be reduced by a factor of two to five, if the cathode is operated in the space charge limited regime rather than in the temperature limited regime.

20. DISTRIBUTION/AVAILABILITY OF ABSTRACT	21. ABSTRACT SECURITY CLASSIFICATION
☒ UNCLASSIFIED/UNLIMITED ☐ SAME AS RPT. ☐ DTIC USERS	UNCLASSIFIED
22a. NAME OF RESPONSIBLE INDIVIDUAL Y. Y. Lau	22b. TELEPHONE (Include Area Code) (202) 767-2765 22c. OFFICE SYMBOL Code 4790

DD FORM 1473, 84 MAR 83 APR edition may be used until exhausted. All other editions are obsolete.

SECURITY CLASSIFICATION OF THIS PAGE

CONTENTS

EFFECTS OF CATHODE SURFACE ROUGHNESS ON THE QUALITY OF ELECTRON BEAMS

I. Introduction

A critical factor in the operation of coherent radiation sources such as free electron lasers (FEL), gyrotrons, etc., is the quality of the electron beams.[1-5] It has been known for some time that the beam quality is limited by the following factors:[6-9] the electron thermal velocities which accompany the finite cathode temperature, the roughness on the cathode surfaces, patchiness and non-uniform emission, asymmetries and non-uniformities in the confining fields, non-adiabatic fields, space charge fields, non-linear forces, etc. Among these, the thermal velocities are considered unimportant for gyrotrons and FELs driven by induction accelerators.[6-8] Non-uniform and non-adiabatic fields may be considerably reduced with careful gun design.[6-9] Space charge effects may be corrected by the well-known Pierce method, at least for one set of parameters. It then appears that the problems which are cathode-related such as patchiness, non-uniform emission, roughness, and non-constant work function, etc., may in many cases place a fundamental limit on the brightness of an electron beam.[9,7] In this paper, we seek to provide some preliminary assessment of the effects of surface roughness on the beam quality. Analytic scaling laws are derived which yield the upper bound on the beam emittance[10-13] in terms of the roughness scales, for both temperature limited and space charge limited regimes.[14] These scaling laws have been supported by numerical integration of the electron trajectories.

Manuscript approved July 7, 1986.

Velocity spread due to surface roughness has been studied previously for the temperature limited regime. Tsimring[6] estimated that surface roughness of 5 μm size may lead to a 5 per cent velocity spread in magnetron injection guns. More recently, Kapetanakos[7] estimated that a fifty micron roughness may result in a normalized emittance of 0.25 cm-rad for a cathode of 5 cm radius. These estimates pointed to the significance of surface roughness on the performance of an electron beam. Both Tsimring and Kapetanakos conjectured that the deleterious effects of surface roughness may be reduced if the cathode is operated in the space charge limited regime. It is these earlier speculations, together with the pressing need to address the beam quality issue, which prompted the more detailed study to be reported in this paper.

Here, we shall only consider non-immersed cathodes, where the external magnetic field is absent. Since the surface roughness has a typical dimension on the order of tens of microns (or less), it is anticipated that its influence on the electron trajectories will be limited to a distance on the order of a few times this dimension, over which the self-magnetic field of the electron beam may certainly be ignored. Thus, magnetic field effects are ignored altogether in the present study and the beam tranverse velocities are caused only by the electrostatic fields. This observation provides considerable simplification. For example, it allows a two-dimensional formulation. As a result, a reliable, yet tractable solution in the temperature limited regime may be constructed.

In the temperature limited regime, the space charge effects are negligible. The electrostatic field is simply the vacuum field which may be readily solved by conformal mapping if a convenient, two-dimensional model is used to represent a rough surface. The electron trajectories subject to this vacuum field may be routinely computed numerically. A scaling law may be regarded as reliable if it agrees with numerical computation over a wide range of parameters.

Matters are substantially more complicated in the space charge limited regime, where the space charge density is highest near the cathode surface. An accurate assessment of the effects of surface roughness would have required, at a minimum, a two-dimensional solution of the Child-Langmuir type over a bumpy suface. Such a solution necessarily reflects the self-consistency between charge distribution and electron trajectories, and an analytic solution does not seem to have been constructed. It is not the objective of this paper to construct such a solution. Rather, we attempt to provide a semi-quantitative answer--based on what we believe to be a reasonable procedure--as to what extent the space charge limited operation would alleviate the surface roughness problem. Essentially, we used the one-dimensional Child-Langmuir field, mapped it onto the bumpy surface as the lowest order approximation, and then calculate the electron trajectories subject to this transformed field. Note that this transformed field, while it is not consistent with the trajectories, does preserve certain expected properties. A scaling law is next constructed and compared with numerical integration based on the procedure. Agreement is observed. But this agreement does not eliminate the possibility that our analysis of the space charge limited regime may be of limited validity so that the resulting scaling law should be regarded as tentative. However, one estimate shows that the error committed is on the order of thirty per cent.

The result of the present study is summarized as follows. The transverse momentum caused by surface roughness is computed numerically and estimated analytically. The maximum values are approximately given by Eqs. (15) and (16), respectively for the temperature limited and space charge limited regime. These formulas have been favorably tested against numerical computation over a wide range of parameters. From these calculations, we conclude that the beam emittance, due to surface roughness alone, is lower for

space charge limited operation than for temperature limited operation by a factor of two to five.

The scaling laws (15), (16) provide an immediate assessment of the effects of surface roughness. An example suffices to illustrate the order of magnitude. For an anode-cathode voltage drop of 250 keV over a distance of 5 cm, say, surface roughness of 5 μm size leads to an equivalent maximum transverse temperature of 10 eV if the cathode is operated in the temperature limited regime, but of 0.55 eV in the space charge limited regime. Since these equivalent temperatures are considerably higher than the normal operating temperature of cathodes, surface roughness (and perhaps cathode patchiness and non-uniform emission) deserves attention in those cases where thermal effects are considered serious. On the other hand, in most existing induction accelerators, surface roughness alone is unlikely to be the only deciding factor in the emittance of a post-accelerated electron beam.

In Section II, we describe the model in more detail and present the results for the temperature limited regime. In Section III, the space charge limited regime is examined. The analytic scaling laws are derived in Section IV, and the concluding remarks will be given in the last section. Some technical details are outlined in the Appendices.

II. The Model and the Temperature Limited Regime

Consider a cathode surface whose roughness is characterized by height h, width w and separation L [Fig. 1, Top]. If L >> h, w, the bumps on the rough surface are uncorrelated and we can consider the emission of a single bump [Fig 1, Bottom]. For simplicity, we consider a two-dimensional model of the protusion, whose profile is described by the equation

$$y = b\left[1 + \frac{a^2}{b^2 + x^2}\right]^{1/2} - b. \tag{1}$$

Here, a and b are constants depending on the height h and w, the full width at half maximum. The relation between a, b and h, w is given in Appendix A. The choice of Eq. (1) for the surface is motivated by the simple transformation $f(z) = (z^2 + 1)^{1/2}$ where $z = x + iy$. [See Appendix A].

Of interest is the degree of divergence of an electron emitted from the rough surface described in Eq. (1). Assuming that the anode is located at $y = D$, where $D >> h, w$, the vacuum electric field E_x, E_y is approximately given by the expression [See Appendix A]

$$E_x + iE_y = \frac{-iE_o\,[x - i(y + b)]}{[(a^2 - (y + b)^2 + x^2) - 2ix(y + b)]^{1/2}}. \tag{2}$$

Equation (2) is valid if the space charge effect is negligible. Here, E_o is the average electric field ϕ/D, ϕ is the anode-cathode voltage drop. The instantaneous position (x,y) and the normalized instantaneous momentum (p_x, p_y) are governed by the following equations

$$\frac{d}{dt}\begin{pmatrix} p_x \\ p_y \end{pmatrix} = \frac{e}{m_o c}\begin{pmatrix} E_x \\ E_y \end{pmatrix} \tag{3}$$

$$\frac{d}{dt}\begin{pmatrix} x \\ y \end{pmatrix} = c\begin{pmatrix} \beta_x \\ \beta_y \end{pmatrix} = \frac{c}{(1 + p_x^2 + p_y^2)^{1/2}}\begin{pmatrix} p_x \\ p_y \end{pmatrix}. \tag{4}$$

If an electron is emitted with zero velocity the initial conditions at time $t = 0$ are:

$$\begin{aligned} x &= x_o\,(u_o) \\ y &= y_o\,(u_o) \\ p_x &= 0 \\ p_y &= 0. \end{aligned} \tag{5}$$

In these equations, e is the electron charge, m_o is the electron rest mass, c is the speed of light, $c\beta_x$, $c\beta_y$ are the components of the instantaneous velocity of the electron, $p_x = \gamma\beta_x$, $p_y = \gamma\beta_y$ with $\gamma = (1 + p_x^2 + p_y^2)^{1/2}$ being the relativistic mass factor, and u_o in Eq. (5) signifies the location on the surface from which an electron is emitted. [See Eqs. (A3), (A4) of Appendix A]

Once E_o, h, w are specified, the field profile is determined from Eq. (2) and (x, y, p_x, p_y) can be numerically integrated in time according to (3), (4) until the electron reaches an energy equal to $E_o D = \phi$. Shown in Figs. 2, 3 are typical numerical results for various electrons as they reach the anode. The transverse displacement $(x - x_o)$ as a function of u_o/u_E is given in Fig. 2 for h = 10 μm, w = 0.1 h, E_o = 0.3 MeV/cm and various values of ϕ. Roughly, u_o/u_E is a measure of the distance along the rough surface from the peak of the bump. More precisely, u_o is defined in Eq. (A3, A4) in terms of (x_o, y_o), the initial position of an electron, $u_o = 0$ corresponds to the peak of the bump and u_E corresponds to a point at the tail of the bump at which $y_o(u_E) = h/10$. [See appendix A]

The data may be understood as follows. Higher values of ϕ imply a larger value of γ and therefore a larger value of $\gamma\beta\ (x - x_o)$ as shown in Fig. 2. Note, however, that $(x - x_o)$ is only weakly dependent on ϕ. Figure 3 shows the value $\gamma\beta\theta$ evaluated at the time when the electrons reach the anode. Here $\theta = v_x/v_y$. At $u_o = 0$, $x_o = 0$, the electric field has no transverse component, therefore $\theta = 0$ as shown in Fig. 3. For $u_o \to u_E$ (i.e., for electrons generated at the tail of the roughness), θ is reduced since the transverse component of electric field is small there. Note that the maximum value of $\gamma\beta\theta$, located at $u_o/u_E = 0.4$ in the case of Fig. 3, is insensitive to ϕ at fixed E_o. This is obvious from Eq. (3):

$$\frac{d}{dt}\ (\gamma\beta\theta) = \frac{dp_x}{dt} = \frac{eE_x}{m_o c} \tag{6}$$

which approaches zero at distances sufficiently far away from the "bump". This constancy of $\gamma\beta\theta$ is consistent with the notion that the emittance is conserved during the acceleration process. The maximum value of $\gamma\beta\theta$, denoted as $\gamma\beta\theta_m$ henceforth, is independent of ϕ (or D). It is this peak value $\gamma\beta\theta_m$ which will be focused in the following, as it provides a measure of the beam divergence due to the surface roughness. In fact, a simple argument would show that its use would yield the upper bound for roughness-induced emittance.

The maximum value $\gamma\beta\theta_m$ depends on h, w and E_o. Shown in Figs. 4-6 is the dependence of $\gamma\beta\theta_m$ on each of these parameters, with the remaining two parameters being held fixed. The range of these parameters is extended arbitrarily so as to compare the numerical result with the scaling laws to be derived later. In Fig. 4, we fix E_o and h on each curve. The decrease in $\gamma\beta\theta_m$ as w increases is expected since enlarging w would reduce the transverse component of the electric field. As $w \ll h$, the horizontal component of the electric field reaches a finite value near the protusion, so does $\gamma\beta\theta_m$ for

small w. On the curves in Fig. 5, both E_o and w are held fixed, the maximum value $\gamma\beta\theta_m$ increases with h for two reasons: (a) the transverse component of the electric field increases with h. (b) More importantly, the spatial extent of the non-uniform field increases with h, thus the electrons receive transverse acceleration for a longer time, leading to a larger value of $\gamma\beta\theta_m$. The increase of $\gamma\beta\theta_m$ with E_o, as shown in Fig. 6, is expected simply because of the larger transverse acceleration associated with increasing E_o. Also shown in the dashed curves in Figs. 4-6 is the value of $\gamma\beta\theta_m$, calculated according to the analytic formula (15) given below. It is seen from these figures that the analytic and numerical results have reasonable agreement over a wide range of parameters, (even beyond those for normal operation). The analytic dependence of $\gamma\beta\theta_m$ on h, w, E_o will become transparent in Section IV.

III. Space Charge Limited Regime

It is of interest to determine the divergence of the electron beam in the space charge limited regime, using the same model of the surface roughness as in the previous section. However, as remarked in the Introduction, this is a rather difficult task if the trajectories of the electrons and the resulting space charge distribution are to be solved consistently over a bumpy surface. Analytic solutions of the Child-Langmuir type over a protrusion do not seem to have been found. Not seeking to construct the Child-Langmuir solution, we attempt to provide instead a rough estimate of the effects of space charges on the divergence of the electron beam, having in mind the construction of a scaling law to compare with the temperature limited regime.

It is natural to use conformal mapping to analyze the space charge limited regime: We first use the space charge limited electric field distribution over a flat surface. We next transform this electric field onto the rough surface using the conformal transformation and then calculate the electron trajectories subject to this field. Note that several properties of the Child-Langmuir field are retained in this procedure: (a) The electric field remains normal to the conducting surface, (b) The electric field varies as $S^{1/3}$ near the surface, as in the Child-Langmuir distribution. Here, S is the distance from the rough surface in the normal direction, and (c) In the limit $h \to 0$, the bumpy surface approaches a flat surface and the solution reduces to that of a one-dimensional Child-Langmuir flow which is truly a consistent solution.

Obviously, the trajectories so constructed cannot be consistent with the charge distribution from which they are computed. For example, the electron trajectories in the one-dimensional Child-Langmuir flow do not intersect, whereas on a rough surface, the electron trajectories may do so. However, one may envision that the procedure described in the preceding paragraph as a

first step in the iterative process: First, use the one-dimensional Child-Langmuir electric field distribution over a flat (u,v) plane and transform it onto the bumpy surface [(x,y) plane] as a first approximate solution. Calculate the electron trajectories over the bumpy surface subject to this transformed Child-Langmuir field. [This is what is done here.] The next round of iteration would be to obtain the electron density from these trajectories, and solve the Poisson equation for the electric field distribution over the bumping surface due to such a charge distribution. This electric field distribution is a next approximation and will be used to re-compute the electron trajectories and the iteration process repeats. Of course, there is no guarantee that such a procedure should converge at all. Should the iteration process converge, what we are calculating is the lowest order approximation. [In fact, even if this procedure can be proven divergent, the result from the lowest order iteration outlined above may still yield useful information--a feat familiar in asymptotic processes.] To assess the errors committed with the use of this method, toward the end of this section, we estimate that the bounds on emittance which we established probably commit an error on the order 30%, or less, over a wide range of parameters.

With this caveat, we again consider a bumpy surface described by Eq. (1) and proceed to numerically integrate the electron trajectories according to (3), (4), subject to the initial conditions (5). The only modification is in the electric field (E_x, E_y) in Eq. (3). According to the procedure outlined in the previous paragraph, it can be shown [Eq. (B21) of Appendix B] that E_x and E_y are given by:

$$E_x = \Lambda(-(v + b)x + u(y + b))/[(x^2 + (y + b)^2)(u^2 + (v + b)^2)]^{1/2}$$

$$E_y = \Lambda(ux + (v + b)(y + b))/[(x^2 + (y + b)^2)(u^2 + (v + b)^2)]^{1/2} \quad (7)$$

under the assumption that E = 0 on the rough surface (space charge limited regime). Here, u and v are functions of x,y defined by the transformation (A1), and

$$\Lambda = \left(\frac{m_o c^2}{e}\right) 2 \frac{Q}{D} Z\left(\frac{Q}{D} v\right). \tag{8}$$

In Eq. (8),

$$Q = 0.61 \times \left[\frac{JD^2}{(1\,kA)}\right]^{1/2} = 0.93 \times (\phi/1\ \text{MeV})^{3/4} \tag{9}$$

is a dimensionless parameter and the function Z(f) is the inverse of the function f(Z), defined by

$$f = \int_0^Z dt\ t^2(1 + t^4)^{-1/2}. \tag{10}$$

The current density J in Eq. (9) is related to the anode-cathode voltage drop ϕ [See Appendix B]. The approximate formula for Q given in the last expression of Eq. (9) is accurate to within 5 per cent for all $\phi \leq 3$ MeV. [For $\phi \geq 3$ MeV, Q may be approximated by $(1 + \phi/.511\ \text{MeV})^{1/2} - 0.8473$, See Appendix B].

The dependence of $(x - x_o)$ and $\gamma\beta\theta$ on u_o as the electrons reach the anode, in the space charge limited regime, is similar to Figs. 2, 3. However, since the thickness of the space charge layer depends on ϕ (or J, or the density) in the space charge limited regime, the peak value $\gamma\beta\theta_m$ depends on four parameters h, w, ϕ, D, instead of three. Shown in Figs. 7-10 are the dependence of $\gamma\beta\theta_m$ on each of these parameters, fixing the remaining three on each curve. Also shown in these figures are the analytic estimates for $\gamma\beta\theta_m$ according to Eq. (16) to be derived in the next section.

Note from Figs. 7, 8 that the dependence on h and w are similar to those in Figs. 4, 5. The slight decrease of $\gamma\beta\theta_m$ with increasing ϕ at fixed $E_o = \phi/D$ [Fig. 9] stems from the fact that higher voltage means larger anode-cathode separation and, as a result, the region of low electric field extends to a larger distance from the cathode. Thus, the effect of the bump, near which the electric field is low, is reduced. This is also reflected from the curves on Fig. (10, right). The remaining features of these curves may readily be understood in a qualitative manner as in the temperature limited regime and will not be repeated here. Note that $\gamma\beta\theta_m$ shown in Figs. 7-10 is lower than the corresponding ones in the temperature limited regime. Note further that the analytic formula yield reasonable agreement with the numerical results.

Let us now return once more to the error inherent in our method. One rough estimate is via the Poisson equation

$$\frac{\partial^2\phi}{\partial x^2} + \frac{\partial^2\phi}{\partial y^2} = \frac{en}{\epsilon_o} = \left|\frac{\partial(u,v)}{\partial(x,y)}\right|^2\left(\frac{\partial^2\phi}{\partial u^2} + \frac{\partial^2\phi}{\partial v^2}\right). \tag{11}$$

Here, we see that solving the Poisson equation in one plane (u,v plane) and transforming the field in another plane (x,y plane) would commit an error on the order of $1-J$, where $J = \left|\partial(u,v)/\partial(x,y)\right|^2$, the square of the Jacobian. We have evaluated J along the trajectory of the electron which yields $\gamma\beta\theta_m$. Fixing h = 10 μm, we found that J ranges between 1 and 1.04 for w = 10 h, between 1 and 1.16 for w = h and between 1 and 0.72 for w = 0.1 h. Thus, it is plausible that the numerical value for $\gamma\beta\theta_m$ computed here, according to numerical or the analytical scaling laws, are accurate to within 30% for all $h/w \leq 10$ compared with a consistent two-dimensional solution of the Child-Langmuir type.

IV. Analytic Scaling Laws:

A ready assessment of the effects of surface roughness may be obtained if the analytic dependence of $\gamma\beta\theta_m$ is given in terms of h, w, ϕ and D. From such scaling laws, a comparison between temperature and space charge limited regime is immediate, at least within the confines of the present model. Such scaling laws for both regimes are now derived.

First, $\gamma\beta\theta$ reaches a constant value at a distance sufficiently far away from the bump, where $E_x \tilde{=} 0$ [cf. Eq. (6)]. Call that distance L_x. Take $L_x = h$. Since the extent of the bump is typically small, we write

$$\gamma\beta\theta \tilde{=} \beta\theta = p_x = v_x/c. \tag{12}$$

The transverse velocity v_x picked up by the action of the horizontal electric field over a distance L_x is approximately given by

$$v_x^2 = 2 \times \text{Acceleration} \times L_x \propto E_n \frac{h}{(h^2 + w^2)^{1/2}} L_x \tag{13}$$

where E_n is the normal component of the electric field. In Eq. (13), we take the directional cosine between the normal and the x component to be $h/(h^2 + w^2)^{1/2}$. Inserting (13) into (12), with $L_x = h$, we have

$$\gamma\beta\theta \propto \sqrt{E_n} \frac{h}{(h^2 + w^2)^{1/4}} \tag{14}$$

where the proportionality constant in (14) is determined by a "one-point fit" with the numerical solution.

For the temperature limited regime, we take $E_n = E_o = \phi/D$ and fix the proportionality constant to write (14) as

$$\gamma\beta\theta_m = 0.15 \sqrt{E_o} \frac{h}{(h^2 + w^2)^{1/4}} \text{ (rad) (Temp. Ltd.)} \tag{15}$$

where E_o is in MeV/cm, and h,w in 100 μm. For the space charge limited regime, we assign E_n to be the Child-Langmuir electric field evaluated at a distance h from a flat surface. [cf. Eqs. (B13), (B16)]. Inserting Eq. (B13) into (14) and determining the proportionality constant again by a "one point fit", we have

$$\gamma\beta\theta_m = 0.079 \frac{h^{1/2}}{(h^2 + w^2)^{1/4}} \left(\frac{Qh}{D}\right)^{2/3} (\text{rad}) \quad \text{(Space Charge Ltd)}. \qquad (16)$$

Here Q is given by Eq. (9) approximately. The scaling laws (15), (16) have been represented by the dotted curves in Figs. 4-10. The agreement between the analytic scaling law and the numerical calculation suggests that the latter is, in fact, valid as long as $E_n \propto S^{1/3}$ near the rough surface for the space charge limited regime. This is the crucial assumption used in the derivation of the scaling law (16). [All other assumptions employed in these scaling laws have been basically verified by noting that in our analysis of the temperature limited regime, for which the scaling law may be taken as reliable, also employ these assumptions. The agreement between the scaling law and numerical integration there provides more confidence on their validity.]

Dividing Eq. (15) by Eq. (16), one may arrive at the following ratio of the emittances for the temperature limited regime and the space charge limited regime, for cathodes of the same size and type:

$$\frac{\varepsilon \text{ (space charge limited)}}{\varepsilon \text{ (temp. limited)}} \simeq 0.51 \left(\frac{h}{D}\right)^{1/6}. \qquad (17)$$

This ratio assumes a value between 0.2 and 0.5 over a wide range of parameters because of the weak 1/6 power dependence in (17). This, perhaps, is a first quantitative assessment of the surface roughness effect in the space charge limited regime. As is evident here, it is supported by extensive numerical calculation.

V. Discussions:

Having derived an analytic scaling law for $\gamma\beta\theta_m$ for an isolated roughness of dimension h, w, one may readily deduce the statistical average $\langle\gamma\beta\theta_m\rangle$:

$$\langle\gamma\beta\theta_m\rangle = \int_0^\infty \int_0^\infty dhdw\ f(h,w)\ \gamma\beta\theta_m \tag{18}$$

where f(h,w)dhdw is the probability of finding a bump of height between h and h + dh, width between w and w + dw. Presumably, f(h,w) is to be determined empirically. The value $R_b\ \langle\gamma\beta\theta_m\rangle$ would then be expected to be the upper bound of emittance of an electron beam of radius R_b, due only to the surface roughness. Simple estimates have, in fact, been obtained by assuming convenient forms of f(h,w) and using Eqs. (15) and (16) into (18).

The next question is whether the emittance due to surface roughness can be measured in experiments. This depends on the resolving power and on the competing effects such as nonlinear space charge and thermal effects. Based on the present study, Loschialpo[13] and Shih[9] showed that surface roughness of 10 μm size can be measured in a two-slit experiment using a 10 kV, 1 A, electron gun with slit width of order 1 mil. The resolving power of such a slit limits the measurable brightness up to a few times 10^7 A/cm^{2}rad^2. Such an experiment is being planned at the Naval Research Laboratory.[7]

We should stress once more that our treatment of the space charge limited regime is only a crude one. Our goal was to provide a lowest order estimate and to propose simple scaling laws. The usefulness of these formulas rests on a direct comparison with an accurate solution (numerical or analytical) of the Child-Langmuir flow over a bumpy surface and, better still, with experiments. A self-consistent, two-dimensional analytic solution of Child-Langmuir type over a rough surface would be highly desirable. It is perhaps of more than academic interest.

While our calculation shows that operation in the space charge limited regime may reduce the deleterious effect of surface roughness, the plasma layer near the cathode surface may be a source of turbulence, whose presence may lead to a marked decrease of the beam quality.

Acknowledgment

I would like to thank C. Kapetanakos, C. W. Roberson, A. Shih, P. Loschialpo, J. Pasour, R. Greene, C. Marrian, R. E. Thomas, L. R. Barnett and S. F. Swiadek for helpful discussions. Valuable suggestions by Sam Penner and Dave Chernin are also gratefully acknowledged. This work is partially supported by ONR and by DARPA under Contract Number 5483.

Appendix A

The Rough Surface and the Vacuum Field Distribution

In this appendix, we consider the electric field distribution over the rough surface for the temperature limited regime. Consider first the conformal transformation $\zeta = f(z)$, defined by

$$\zeta = u + iv = [(z + ib)^2 + a^2]^{1/2} - ib \tag{A1}$$

where $z = x + iy$ is the complex variable and a,b are real, positive constants reflecting the height h and width w of the surface roughness. From (A1), it can be shown that the $v = 0$ axis of the $\zeta = u + iv$ plane is mapped onto the contour

$$y = b\left[1 + \frac{a^2}{b^2 + x^2}\right]^{1/2} - b \tag{A2}$$

in the x,y plane. Equation (A2) is used to model the roughness and is reproduced in Eq. (1) of the main text. Various points on the $v = 0$ axis of the ζ plane map onto the cathode surface modelled by Eq. (A2). Thus, we may use u_o to parametrize the points (x_o, y_o) of electron emission. In terms u_o, we obtain from Eqs. (A1) and (A2):

$$y_o = -b + (1/\sqrt{2})\left\{-(u_o^2 - a^2 - b^2) + [(u_o^2 - a^2 - b^2)^2 + 4u_o^2 b^2]^{1/2}\right\}^{1/2} \tag{A3}$$

$$x_o = u_o b/(y_o + b). \tag{A4}$$

Similarly, we may use u_E to designate the point (x_E, y_E) on the tail of the "bump" at which $y_E = 0.1\ h$, where h is the height of the bump given by [cf. Eq. (A2)]

$$h = (b^2 + a^2)^{1/2} - b. \tag{A5}$$

The full width at half maximum, w, is

$$w = 2b \left[\frac{3a^2 + 2b^2 - 2b\,(a^2 + b^2)^{1/2}}{a^2 - 2b^2 + 2b(a^2 + b^2)^{1/2}}\right]^{1/2}. \tag{A6}$$

To find a,b in terms of h,w from (A5) and (A6) would require numerical calculation. The following approximations obtained from (A5) and (A6) may be useful. For $h/w \geq 1$

$$\begin{aligned} a &\simeq h + w/3.464 \\ b &= (w/3.464)[1 + 1/(3.464\ h/w)] \end{aligned} \tag{A7}$$

whereas for $h/w \ll 1$,

$$\begin{aligned} a &= (hw)^{1/2} \\ b &= w/2. \end{aligned} \tag{A8}$$

We have verified that (A7) is accurate to within 2.5 per cent for all $h/w \geq 1$, whereas (A8) is accurate to within 4 per cent if $h/w \leq 0.1$.

With the branch appropriately chosen, ζ is an analytic function of z which maps the upper half ζ plane onto the upper z plane, the latter being bounded below by the contour described in Eq. (A2). Thus a uniform electrostatic field in the upper ζ plane will be mapped into the electrostatic field over the rough surface in the temperature limited regime. Such a transformation is given, for example, in Ref. 15. When applied to the present

model, the electric field (E_x, E_y) in the (x,y) plane reads

$$E_x + iE_y = \frac{-iE_o\,[x - i(y + b)]}{\{[x - i(y + b)]^2 + a^2\}^{1/2}} \qquad (A9)$$

which is rewritten as Eq. (2) of the main text. Here E_o is the (constant) electric field far away from the protrusion. It may be taken as ϕ/D when the dimensions h, w of the bump are much smaller than the anode-cathode separation D.

From the transformation (A1), we may find (u,v) in terms of (x,y). The unit vector $\hat{v}$ in the (u,v) plane is found to be mapped into the vector

$$\hat{v} = \frac{1}{[(u^2 + V^2)(x^2 + Y^2)]^{1/2}}\,\{\hat{x}(-Vx + uY) + \hat{y}(ux + VY)\} \qquad (A10)$$

where $V = v + b$, $Y = y + b$.

Appendix B

One-Dimensional Space Charge Limited Flows

The one-dimensional space charge limited flow (Child-Langmuir flow) serves as a useful reference in the present study. The relativistic formulation was given by Jory and Trivelpiece[16] and is recapitulated briefly below. Let U(s) be the steady velocity of a one-dimensional electron flow in the s direction. The plane s = 0 represents the flat cathode surface. Let J, n(s), and E(s) be the electron current density, electron number density and the electric field, respectively. The governing equations for E(s) and U(s) read

$$U \frac{d}{ds} (\gamma U) = \frac{e}{m_o} E(s) \tag{B1}$$

$$\frac{dE(s)}{ds} = \frac{1}{\varepsilon_o} \frac{J}{U(s)}. \tag{B2}$$

In the force law (B1), $\gamma = (1 - U^2/c^2)^{-1/2}$ is the relativistic mass factor and in writing the Poisson equation (B2), we have used the continuity equation en(s) U(s) = J = constant. Introducing a time-like variable ξ, defined by

$$d\xi = \frac{ds}{U(s)}, \quad \xi = \int_o^s ds/U(s) \tag{B4}$$

we immediately integrate (B2) to obtain

$$E = \frac{1}{\varepsilon_o} J\xi \tag{B5}$$

where we assume E = 0 at the cathode surface (s = ξ = 0).

We next substitute (B5) into (B1) to obtain

$$\gamma U = \int_0^{\xi} d\xi \, \frac{e}{m_o} E = \frac{e}{m_o \epsilon_o} J \frac{\xi^2}{2} \tag{B6}$$

which leads to

$$U = c\eta^2 Q^2 / [1 + \eta^4 Q^4]^{1/2}. \tag{B7}$$

In (B7), both

$$\eta = c\xi / D \tag{B8}$$

and

$$Q = (D/c) \, (eJ/2m_o c\epsilon_o)^{1/2} \tag{B9}$$

are dimensionless. Substitution of (B7) into (B4) yields s as a function of ξ:

$$s(\xi) = (D/Q) \, f \, (cQ\xi/D) \tag{B10}$$

where f(z) is defined as

$$f(z) = \int_0^z \frac{dt \, t^2}{(1 + t^4)^{1/2}} \tag{B11}$$

whose inverse,

$$z = Z(f) \tag{B12}$$

yields ξ as a function of s according to Eq. (B10). [The property of this inverse function Z(f) is described in the next paragraph.] Thus the solution $E(s)$, $V(s) = \int_0^s E(s)ds$, and $p = \gamma U/c = \gamma\beta$ may be founded from (B5), (B7):

$$E = \frac{2m_o c^2}{eD} Q\, Z\, (Qs/D) \tag{B13}$$

$$V = 0.511\ \text{MeV} \times \{[1 + (Z(\tfrac{Qs}{D}))^4]^{1/2} - 1 \tag{B14}$$

$$p = [Z(\tfrac{Qs}{D})]^2. \tag{B15}$$

In Eqs. (B12)-(B15), the function Z(f) assumes the following asymptotic formula which may be established from (B11):

$$Z(f) = \{3f/[1 - 0.9272f^{4/3} + 1.9146f^{8/3}]\}^{1/3},\ f \leq 0.1 \tag{B16}$$

$$Z(f) = f + 0.84731 - 0.16667/(f + 0.84731)^3,\ f \geq 1. \tag{B17}$$

For all f lying in the ranges indicated in (B16) and (B17), these asymptotic formulas are accurate up to 1 part in 10^3. They are more accurate than those given in Ref. 16. The numerical values of Z(f) equal to 0.678, 0.872, 1.022, 1.153, 1.275, 1.390, 1.501, 1.609, 1.715, 1.820 for f = 0.1, 0.2, 0.3, ..., 0.9, 1.0, respectively.

When s = D, V = ϕ, the anode-cathode voltage drop. Thus, Q and ϕ are related according to Eq. (B14):

$$\phi = 0.511\ \text{MeV} \times \{[1 + (Z(Q))^4]^{1/2} - 1\}. \tag{B18}$$

This relation gives the dependence of Q on ϕ and is shown in Fig. 11. Also shown in this figure is the function

$$g(\phi) = Q^{2/3}/(\phi/1\ \text{MeV})^{1/2} \tag{B19}$$

which is almost a constant for all $\phi < 3$ MeV. Thus, to within 5 per cent, this constant is 0.9. A good approximation of Q then reads

$$Q \tilde{=} 0.93\ (\phi/1\ \text{MeV})^{3/4}. \tag{B20}$$

Both Eqs. (B9) and (B20) are reproduced in Eq. (9) of the main text.

Note that all of the well-known properties of the classical Child-Langmuir flow are recovered in the limit of low voltage. For example, using (B16) in (B13), (B14), we have $E \propto s^{1/3}$, $\phi \propto s^{4/3}$, $n \propto dE/ds \propto s^{-2/3}$ near the cathode surface ($s \to 0$).

In Section IV, we used the one-dimensional Child-Langmuir solution in the $\zeta = v + iv$ plane: [cf. (B13)]

$$\vec{E} = \hat{v}\,\frac{2m_o c^2}{eD}\,QZ(Qv/D) \tag{B21}$$

where the unit vector $\hat{v}$ is transformed according to Eq. (A10) of Appendix A.

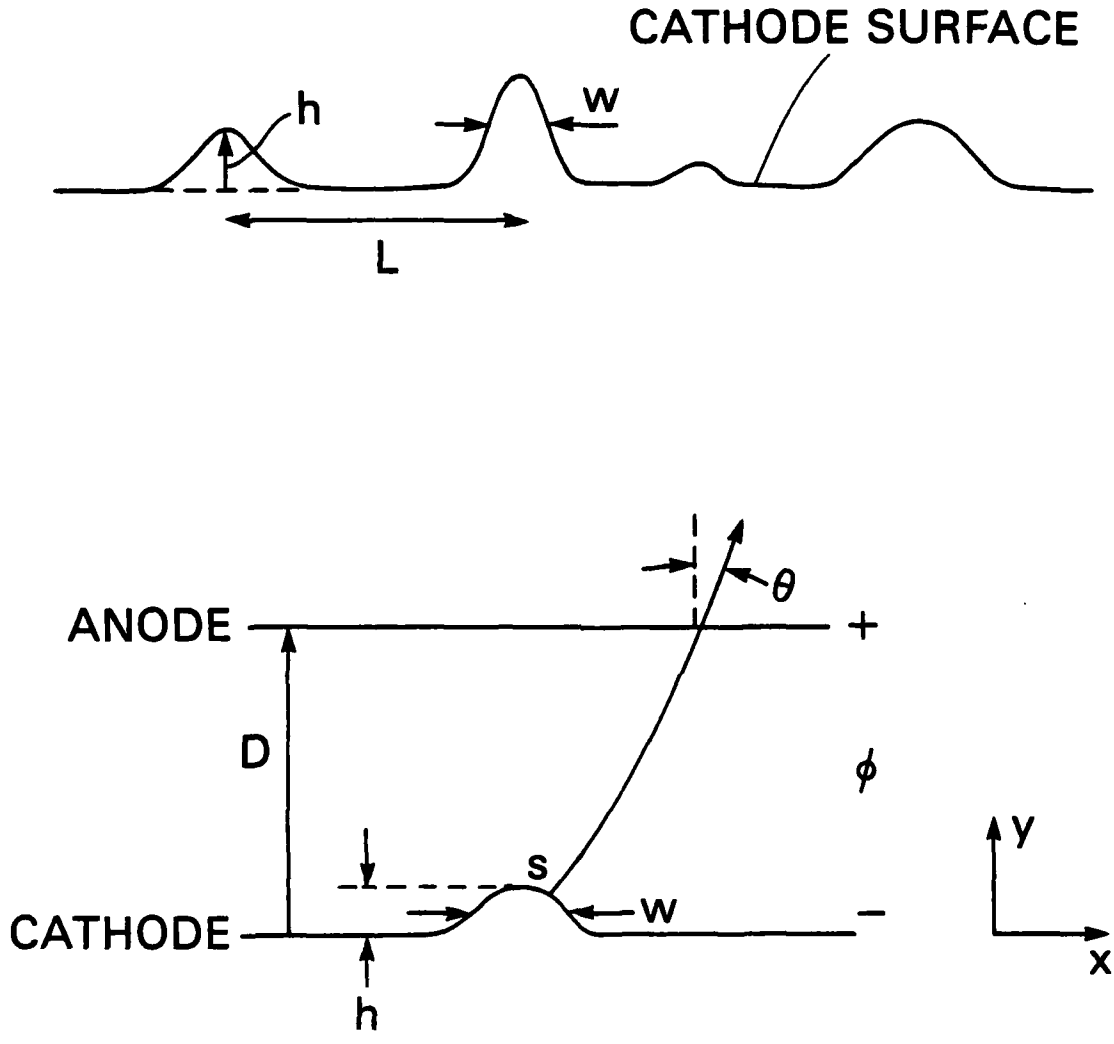

Fig. 1. Schematic drawing of a rough cathode surface.

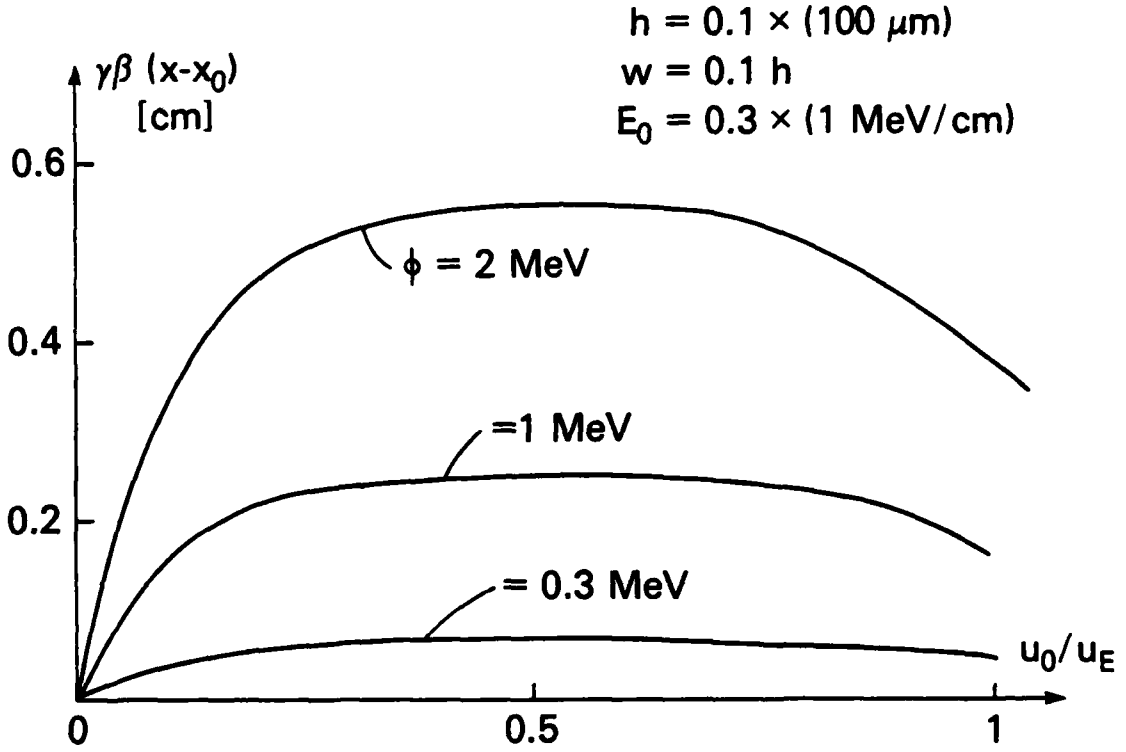

Fig. 2. Transverse displacement $\gamma\beta(x-x_o)$ as a function of u_o/u_E, when the electron reaches the potential specified on the curves. See text for the precise definition of u_o/u_E, which signifies the position on the cathode surface from which the electron is emitted.

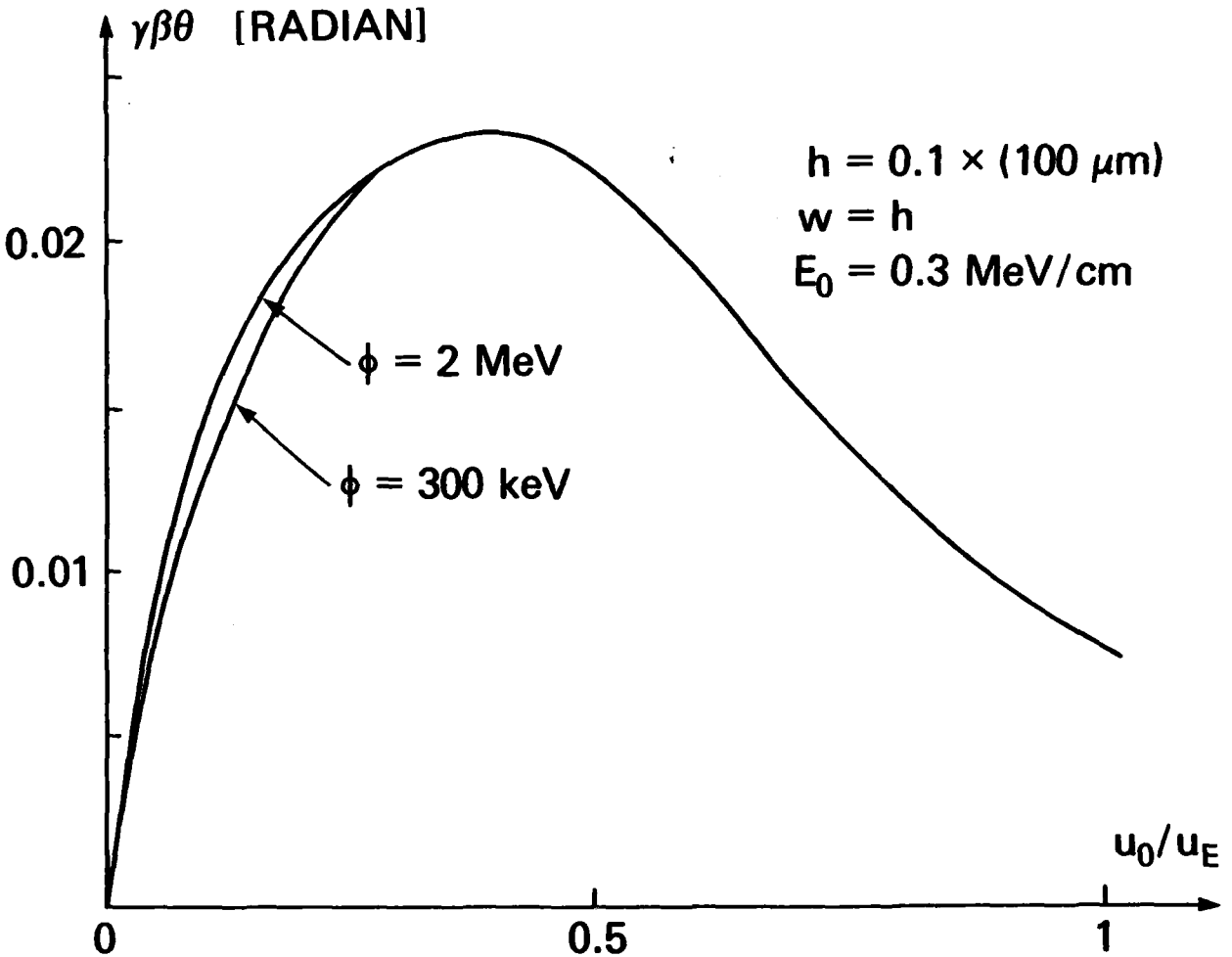

Fig. 3. The amgular displacement βYθ as a function of u_0/u_E when the electron reaches the potential ϕ as specified on the curves.

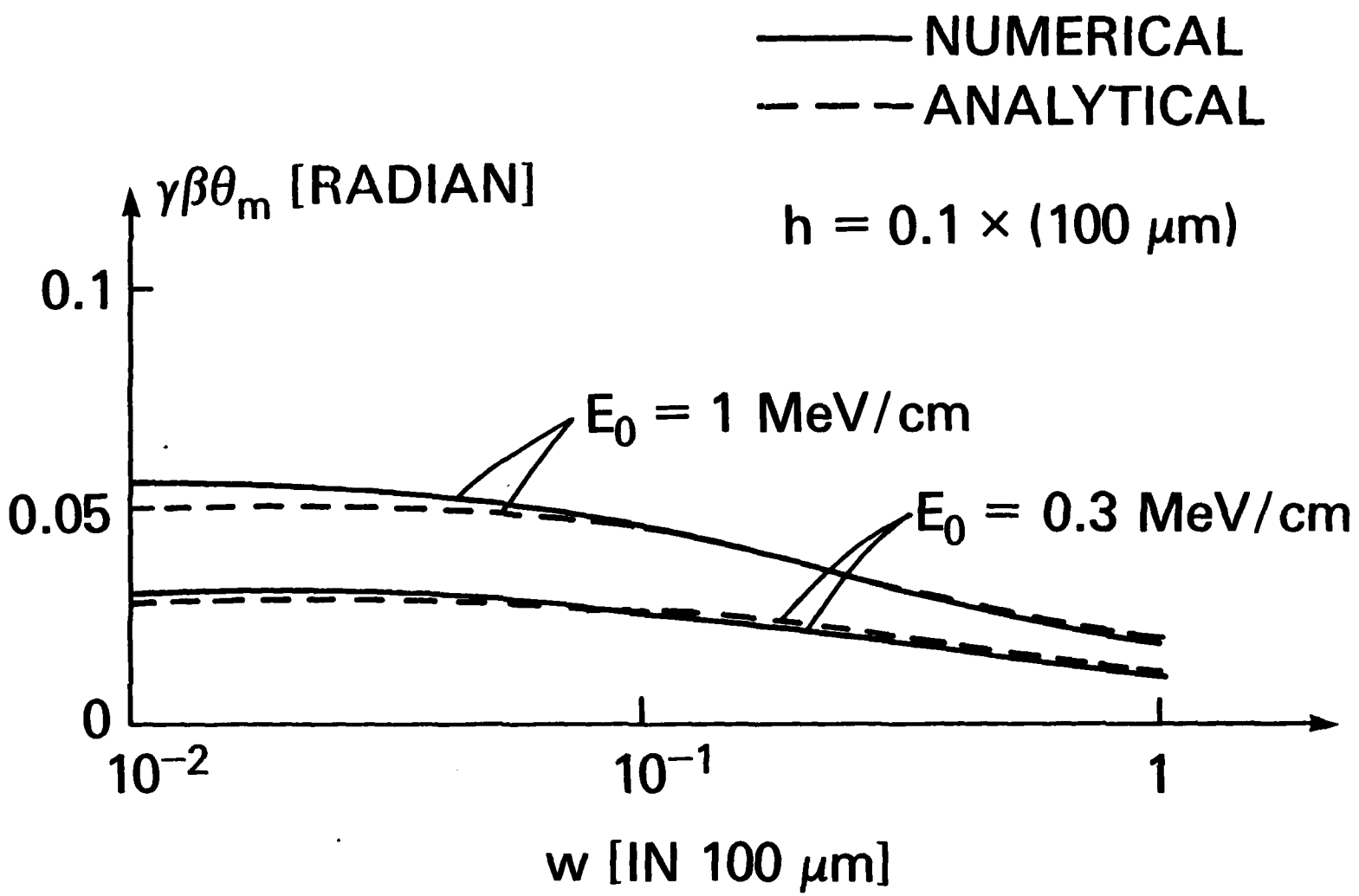

Fig. 4. The peak value $\gamma\beta\theta_m$ as a function of the width w in the temperature limited regime. The analytic results are obtained from Eq. (15).

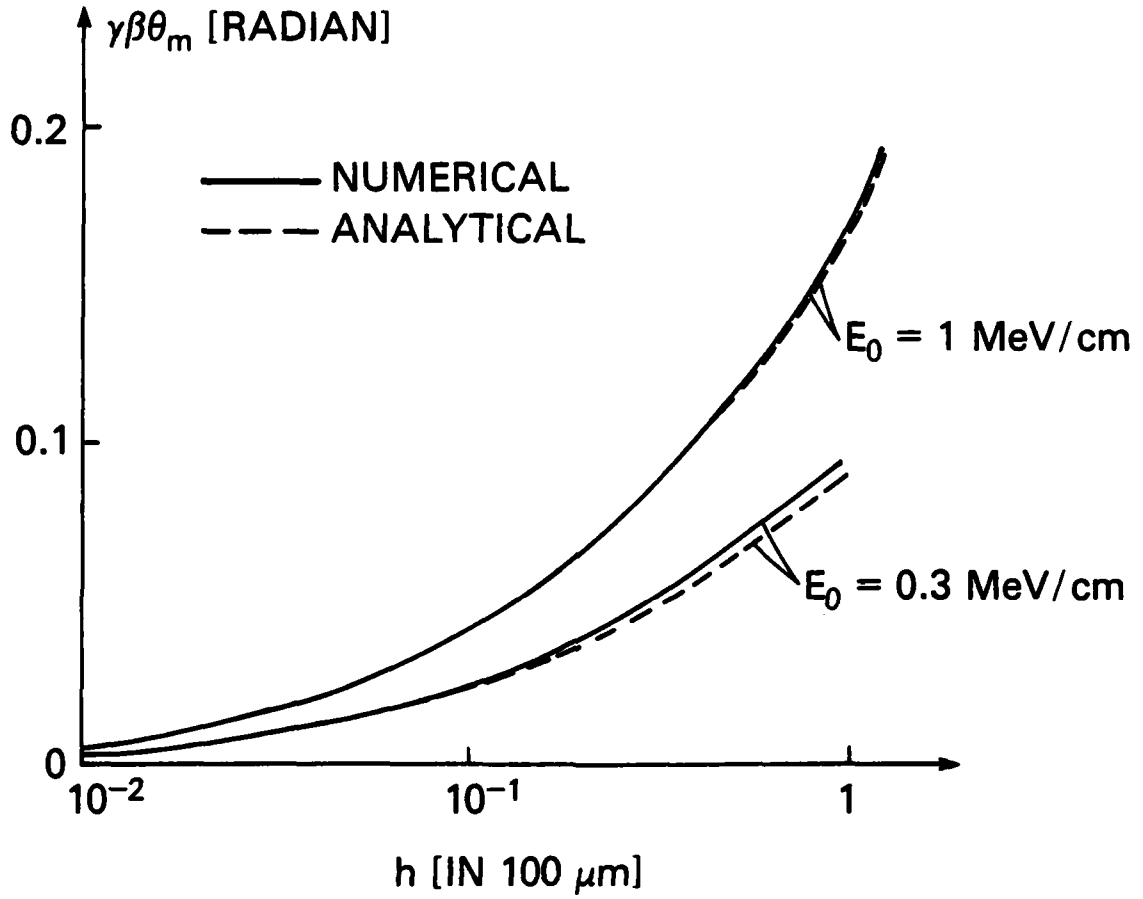

Fig. 5. The peak value $\gamma\beta\theta_m$ as a function of the height h in the temperature limited regime.

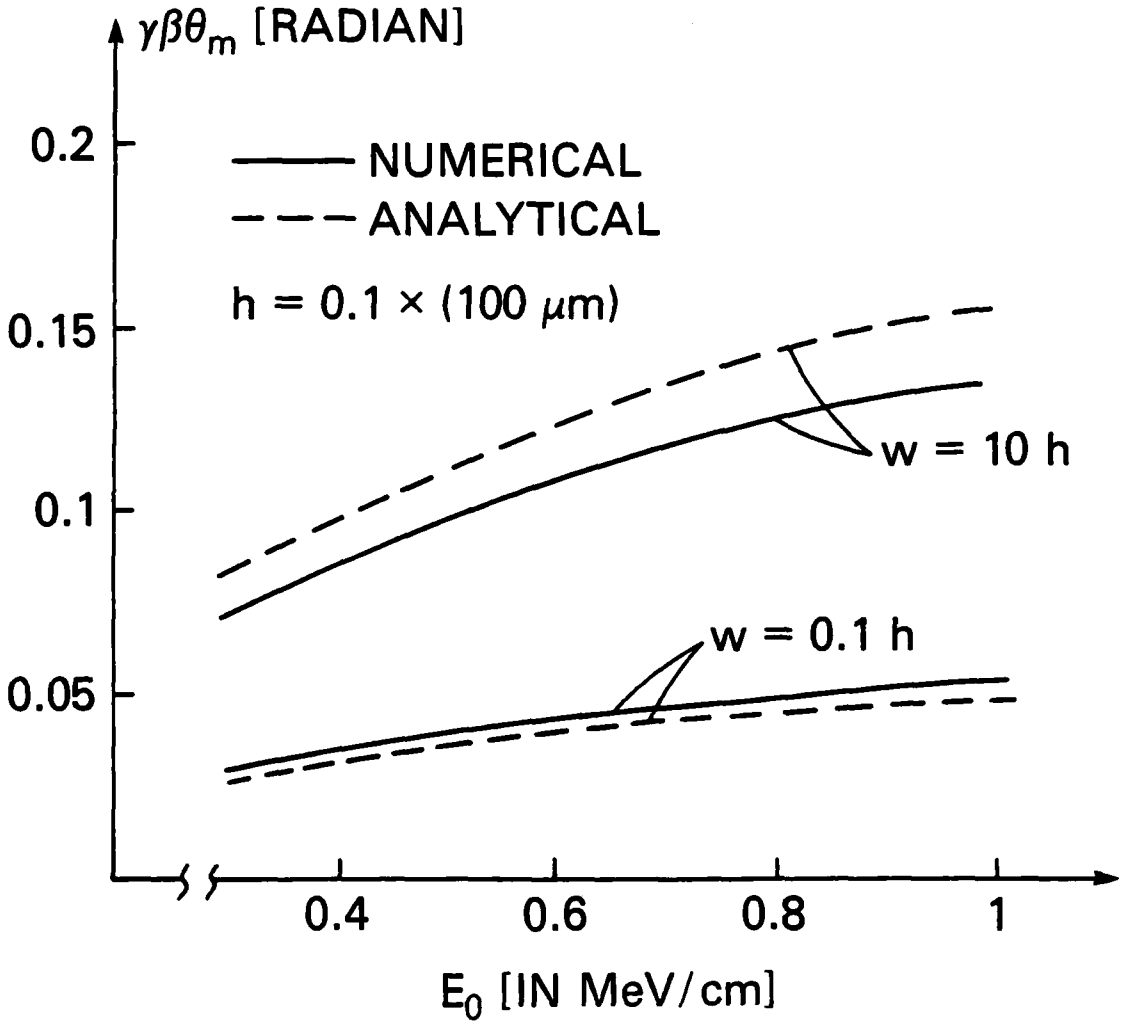

Fig. 6. The peak value $\gamma\beta\theta_m$ as a function of the electric field E_o in the temperature limited regime.

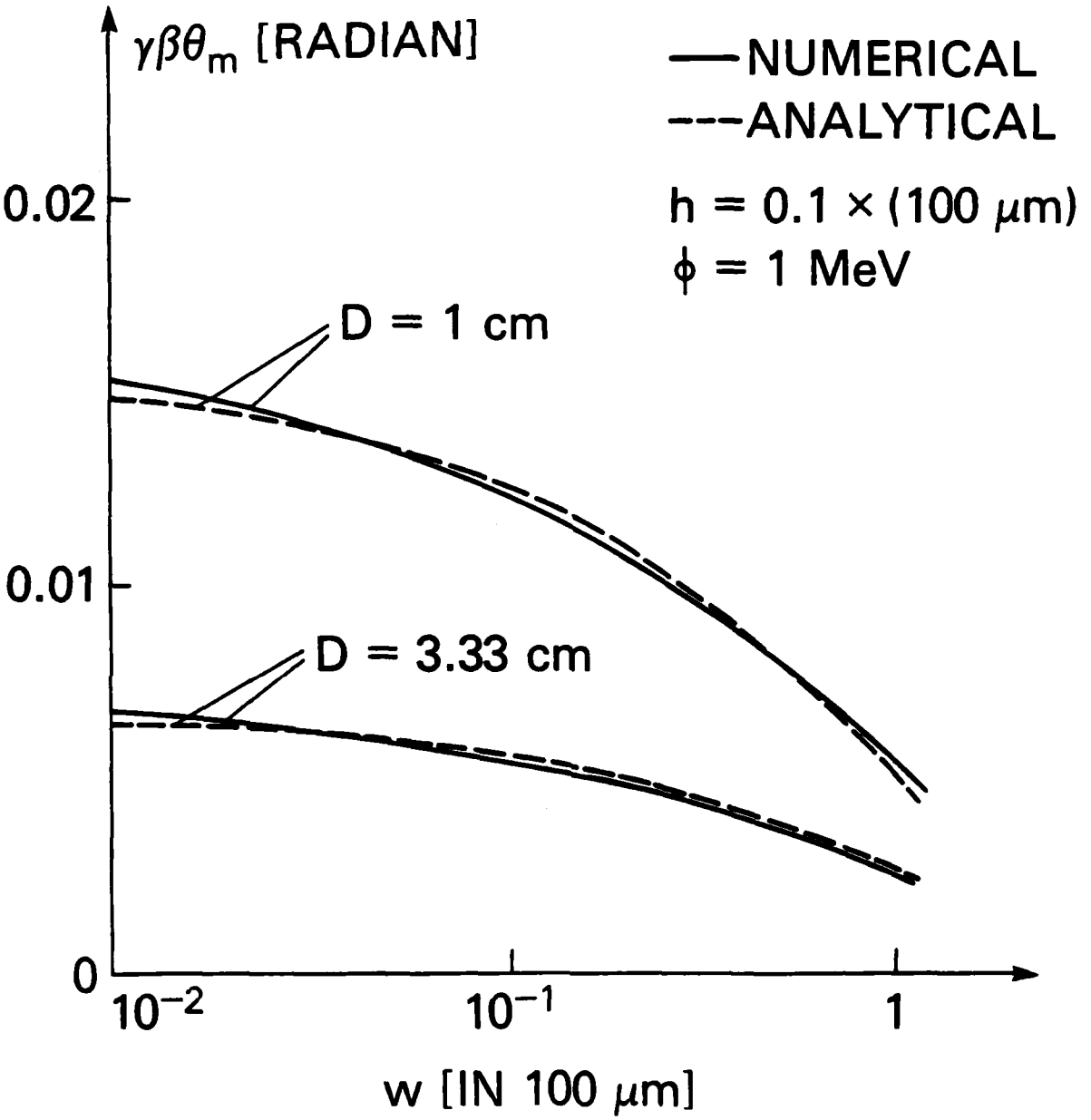

Fig. 7. The peak value $\gamma\beta\theta_m$ as a function of the width w in the space charge limited regime. The analytic results shown in Figs. 7-10 are obtained from Eq. (16).

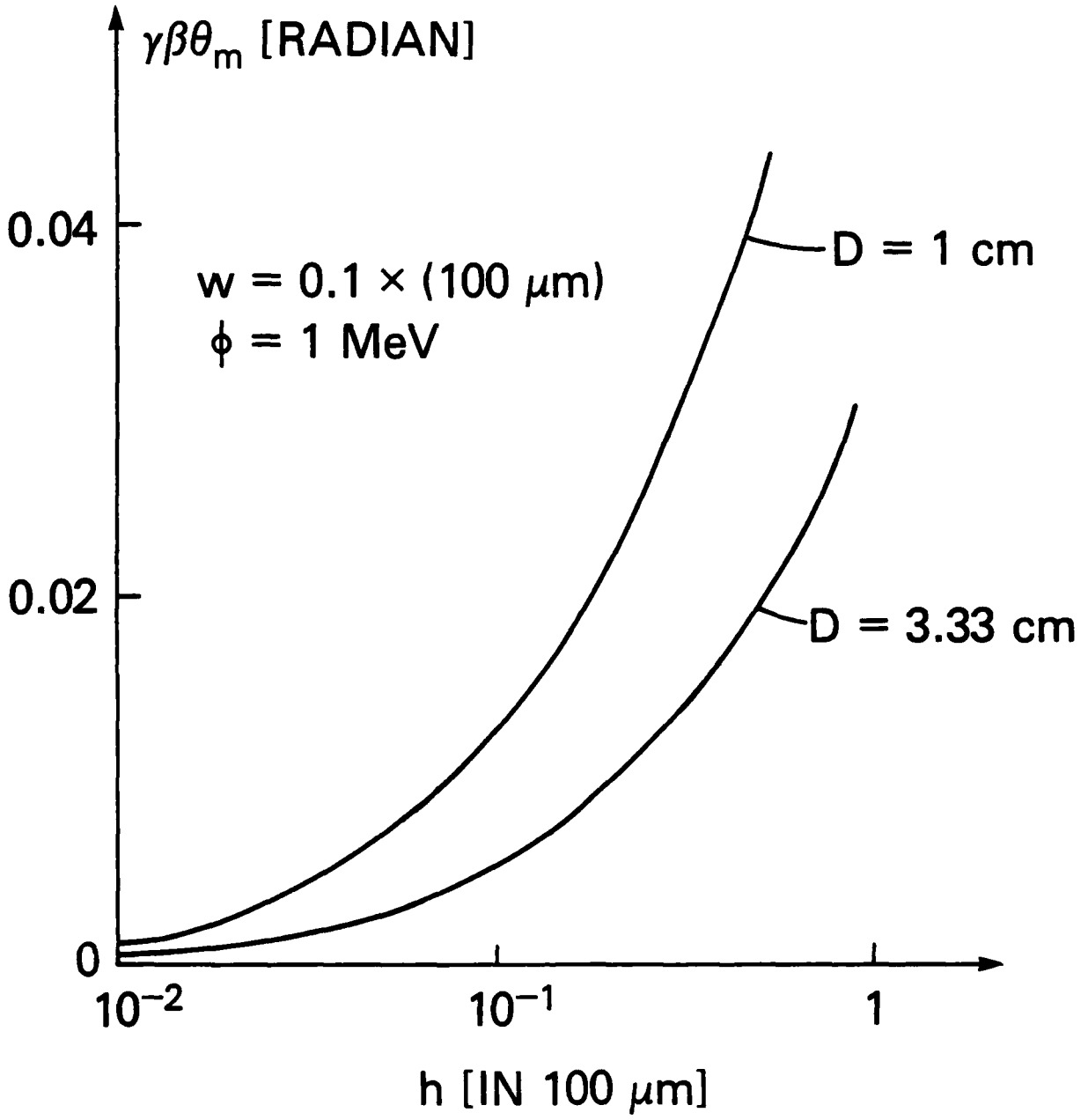

Fig. 8. The peak value $\gamma\beta\theta_m$ as a function of the height h for the space charge limited regime. The analytical and numerical results are practically indistinguishable in this figure.

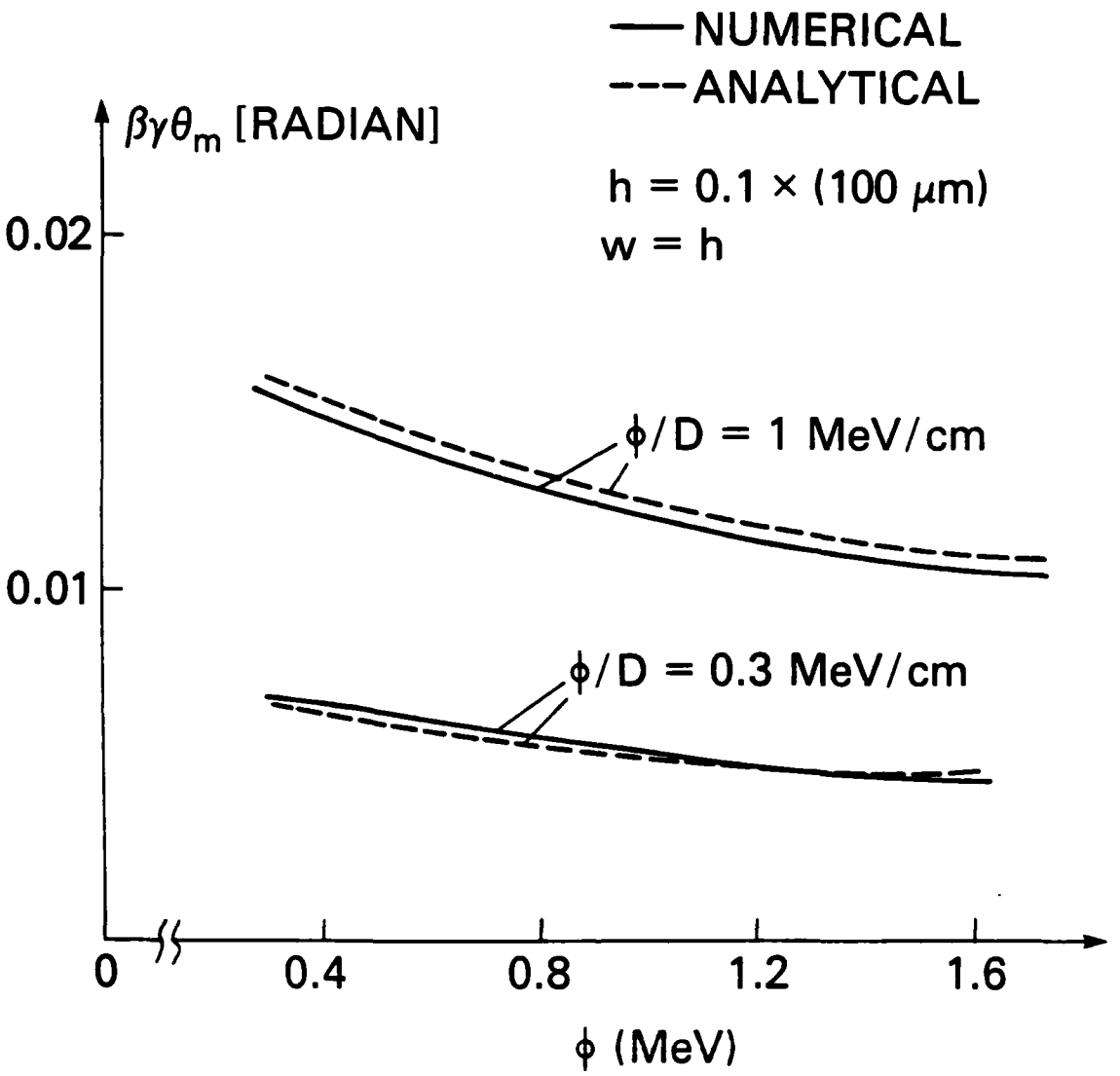

Fig. 9. The peak value $\gamma\beta\theta_m$ as a function of the anode-cathode voltage drop ϕ in the space charge limited regime.

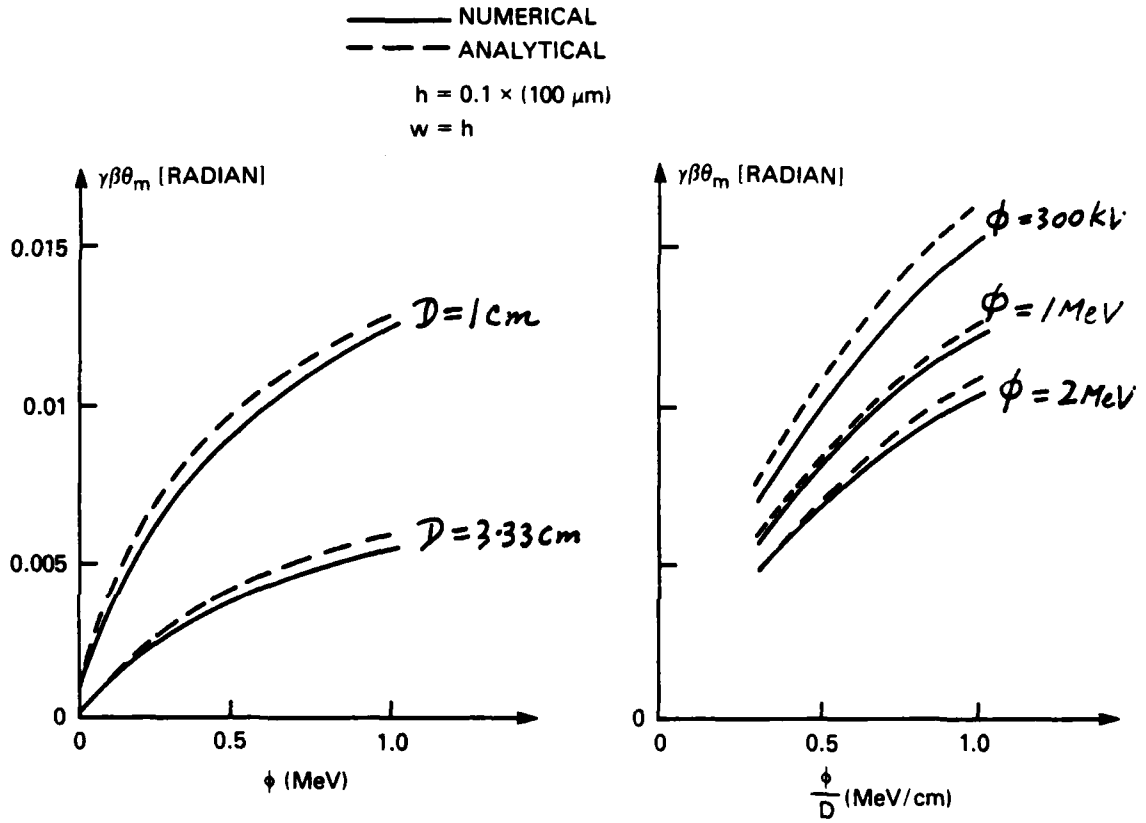

Fig. 10. (Left): The peak value $\gamma\beta\theta_m$ as a function of ϕ for two values of D for the space charge limited regime [compare with Fig. 9].
(Right): The peak value $\gamma\beta\theta_m$ as a function of the average electric field ϕ/D, for the space charge limited regime.

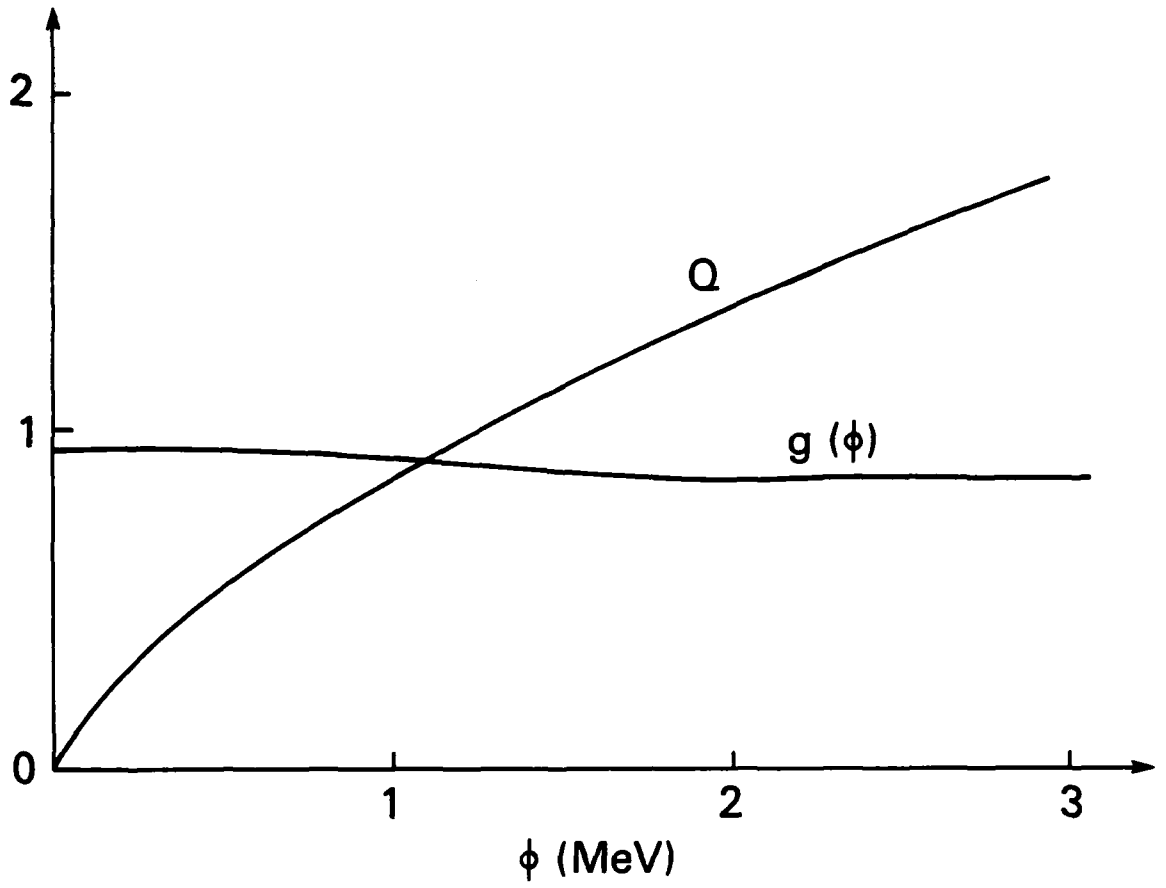

Fig. 11. The dimensionless functions Q and $g(\phi)$ defined in Eqs. (B18) and (B19). Note that $g(\phi)$ is almost constant.

References

1. The precise definition of electron beam quality, which is universally adopted in the literature on radiation devices, is yet to be established. Recently, Roberson (Ref. 2) introduced one which may be of value to free electron laser research. Earlier discussions on electron beam quality, beam brightness, velocity spread, emittance, etc., may be found in Refs. 3-5.

2. C. W. Roberson, IEEE J. Quantum Electronics QE-21, 860 (1985).

3. J. D. Lawson, "The Physics of Charged Particle Beams", (Oxford University Press), p. 182 (1977).

4. C. Lejeune and J. Aubert, in "Applied Charged Particle Optics", ed. A. Septier (Academic Press), Part A, p. 159 (1980).

5. J. Pasour, R. Lucey and C. W. Roberson in: Free-Electron Generators of Coherent Radiation, C. A. Brau, S. F. Jacobs and M. O. Seally, eds., [Proc. Soc. Photo-Optical Instrumentation Eng. SPIE Vol. 453,] p. 328 (1984).

6. S. E. Tsimring, Izv. Radiofizika, Vol. 15, p. 1247 (1972).

7. C. Kapetanakos, private communication (1985).

8. W. Barletta, J.K. Boyd, A.C. Paul, and D.S. Prono, in Proc. 1984 Free Electron Laser Conf. Castelgandolfo, Italy; Sept. 1984.

9. A. Shih, C. Marrian, R. Greene, private communication (1985).

10. The precise definition of electron beam emittance is given in Ref. 4. Some recent measurements of beam emittance are discussed in Refs. 9, 11-13.

11. D. A. Kirkpatrick, R. E. Shefer and G. Bekefi, J. Appl. Phys. 57 5011 (1985).

12. A. C. Paul, A. M. Sessler, J. S. Wurtele, G. J. Caporaso and A. G. Cole, in "Free-Electron Generators of Coherent Radiation", Eds. C. A. Brau, S. F. Jacobs and M. O. Scully, Bellington, WA: SPIE, p, 108 (1983). [SPIE PROC. V. 453]

13. P. Loschialpo, W. Namkung, M. Reiser and J. D. Lawson, J. Appl. Phys. 57, 10 (1985). Also, P. Loschialpo, private communication (1985).

14. Y. Y. Lau, Bull. Am. Phys. Soc. 30, 1583 (1985).

15. F. B. Hildebrand, Advanced Calculus for Applications, (Prentice Hall, NJ, 1962), p. 580.

16. H. R. Jory and A. W. Trivelpiece, J. Appl. Phys. 40, 3924 (1969).